

IMPROVED FUNCTIONALITY AND PERFORMANCE IN PHOTONIC INTEGRATED CIRCUITS

Larry A. Coldren, James Raring, Matt Sysak, Jonathan Barton, and Leif Johansson

Materials and Electrical and Computer Engineering Depts., University of California,
Santa Barbara, 93106

Abstract

With the continued maturation of InP-based photonic ICs, improvements in their functionality, performance, and reliability are evolving. High-performance single-chip transmitters, receivers, sensors, transceivers, and wavelength converters that integrate numerous components have been demonstrated. Here we summarize results of integrated widely-tunable transmitters using two different integration platforms.

I. Introduction

The majority of optoelectronic components comprising modern day communications systems are discrete in nature. Several of these discrete components with differing functions are then interconnected using fiber splices in a configuration to provide the required system functionality. The underlying advantage of this method is that each component is optimized for one specific function, enabling deployment of state of the art components. However, there are several shortcomings involved with this method. The difficulty in efficiently coupling light on and off each discrete chip is great. Advances in the coupling between the semiconductor chip and optical fiber using mode converters is a significant step in reducing the coupling loss, yet coupling is still a dominant source of optical loss. Another draw back to discrete components is the expense involved with packaging each component individually. This is the major expense as devices are taken from fabrication to deployment. A reduction of the packaging cost can be accomplished by using co-packaging of optoelectronic components although device-to-device coupling is still an issue.

The monolithic integration of the optoelectronic devices on a single chip offers the potential to completely eliminate the device-to-device coupling problem. This can provide a significant reduction in packaging cost and package size as well as increased reliability and reduced power dissipation. Increased reliability results from the elimination of possible mechanical movements amongst the elements of an optical train and the reduced driving currents allowed by the reduction in optical coupling loss between elements. The reduction in required drive currents subsequently results in decreased device power consumption.

There are some general requirements that must be fulfilled when monolithically integrating optoelectronic components. First, each integrated component must function as intended. The performance of each integrated component must operate at a level that will enable the PIC as a whole to achieve its specified performance level. Clearly, as these levels are increased, the performance demands of the individual integrated components will also be increased. The second requirement is that the operation of one component must not adversely effect the operation of another. That is, each component should be isolated from the other components on chip and function as if it were discrete. These requirements allow for the design of PICs using an optoelectronic building blocks approach such that discrete components sharing a common growth and processing platform can be combined in a way that creates a higher functionality device or PIC. When implementing a method for monolithic integration, the trade-off between fabrication difficulty and device optimization capabilities should be carefully weighed since added processing steps and growth complexity can lead to increased manufacturing costs and yield reduction. Additionally, the method should not be prohibitively time consuming or expensive. A review of some of some integration methods are given in the following section.

II. Integration Technologies

Three established active-passive integration techniques are outlined in Fig 1. The butt-joint regrowth method is an example of an integration scheme offering a high degree of versatility, because waveguides with exactly the desired properties can be grown successively after removal of the original waveguide¹. However, it tends to suffer from imperfect interfaces between the two guides, resulting in unwanted scattering loss and reflections. Of course, a separate

regrowth is required for each new bandgap or other waveguide property change.

Selective area growth (SAG) uses a dielectric mask to pattern the wafer, which inhibits epi-layer growth during MOCVD². As a result the layers grow thicker near the dielectric mask and this can be used to tailor the waveguide properties along its length. However, waveguide properties cannot be shifted very abruptly, the waveguide thickness and confinement factor also change, and critical control of growth parameters are necessary.

An established and very simple integration platform is based on the use of offset QWs, where the multi-quantum well (MQW) active region is grown above a passive bulk waveguide that extends throughout the PIC³. Passive, tuning, or modulator regions are then formed by selectively etching off the MQW active prior to the single non-critical regrowth. However, here there is a slight discontinuity at the interface, the confinement factor is limited by the offset geometry in the active section, and only two possible waveguides/bandgaps are possible. Nevertheless, this platform has enjoyed commercial success with fairly complex PICs involving, for example, a five-section widely-tunable SGDBR laser, an SOA, and an EAM on a single chip. The SGDBR itself contains two tunable mirrors, a backside detector, an intracavity phase shifter, and a gain region.

In order to improve upon the above well-established integration platforms, two new platforms have been developed as shown in Fig. 2. The first, called the ‘dual quantum-well’ approach, is just like the offset QW platform outlined in Fig. 1 (c), with the addition of higher bandgap QWs in the common ‘passive’ waveguide⁴. This is very beneficial for more efficient electroabsorption and phase modulators due to the possible use of the quantum-confined Stark effect (QCSE), which provides a more abrupt absorption edge. With only a moderate increase in the base structure growth complexity,

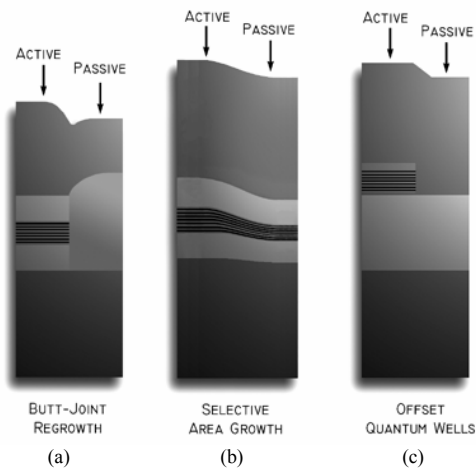


Fig. 1. Various techniques for achieving active and passive sections orthogonal to the growth direction.

QW EAMs can now be realized on the same chip as widely-tunable lasers using the identical simple processing steps as in the offset QW method. This scheme offers a large degree of EAM design freedom since the MQW design can be tailored without disruption of the laser active region. This freedom opens new avenues for the use of specially designed wells for optimum modulator performance in terms of well depth, well/barrier width, and well symmetry.

Another method to realize multiple QW bandedges is through quantum well intermixing (QWI), which allows for the strategic, post growth, tuning of the QW band edge using a relatively simple procedure⁵. This is illustrated in Fig. 2b. As this technique enables the employment of centered MQW active regions for maximized modal gain lasers and blue shifted QWs by various amounts for use in EAMs and passive waveguides. QWI breaks the trade-off associated with the simple fabrication scheme offered by the offset QW method and the design flexibilities offered by butt-joint regrowth and SAG. QWI makes use of the metastable nature of the compositional gradient found at heterointerfaces. The natural tendency for materials to interdiffuse is the basis for the intermixing process. Also, because QWI does not change the average composition, but only slightly changes the compositional profile, there is a negligible index discontinuity at the interface between adjacent sections. This eliminates parasitic reflections that can degrade performance.

In our work we employ the implant-enhanced interdiffusion technique, which relies on the diffusion of point defects created during an ion implantation into an InP implant buffer layer grown above the MQW active region. This method has been shown to have good spatial resolution, and be controllable using anneal time, temperature, and implant dose⁵. Furthermore, we have shown that numerous QW band edges can be obtained by sequential selective removal of the vacancy source followed by a prescribed RTA. As indicated in Fig. 3a the properties of the resulting MQW regions still

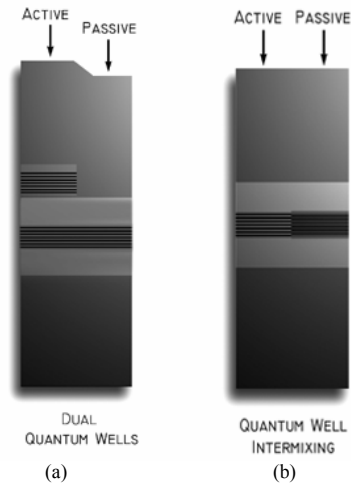


Fig. 2. Newer integration techniques for enhanced high-functionality PIC performance

have good QCSE behavior. And as shown in Fig. 3b low-loss passive waveguides are enabled by shifting the absorption edge further.

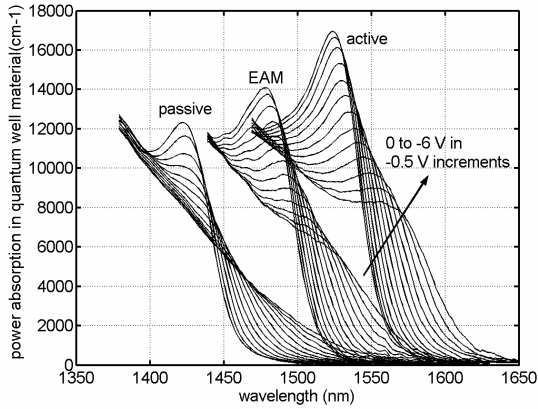


Fig. 3a. Photocurrent vs. wavelength for as grown, partially intermixed (EAM) and more fully intermixed (passive) quantum wells.

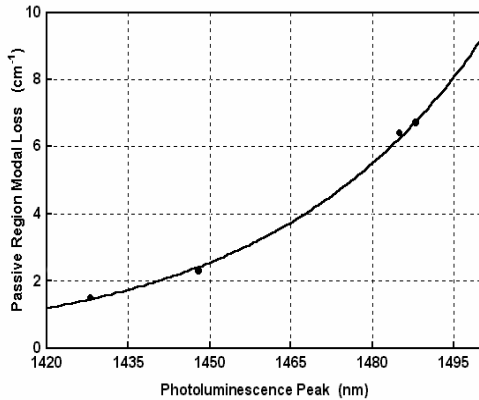


Fig. 3b. Passive region modal loss vs. photoluminescence peak wavelength measured at 1570nm.

III. PIC Results

In the following sections results are presented from PICs fabricated on the dual QW and on the QWI platform. First we report the performance 10 Gb/s widely-tunable transmitters monolithically integrated with photoreceivers employing waveguide flares for both the SOA and the detector for the realization of a 10 Gb/s photocurrent-driven wavelength converter (PD-WC). In the following section results are

shown for a 10 Gb/s widely-tunable negative-chirp transmitter fabricated using QWI.

III.A. Dual QW 10 Gb/s Transmitter with Integrated Receiver

SG-DBR lasers have been integrated with QW EAMs and SOA/QW p-i-n receivers employing flares and tapers for improved saturation characteristics⁶ using the dual QW platform. This device, shown in Fig. 4, was the first single chip widely tunable EAM based 10 Gb/s PD-WC providing 10 dB of output signal extinction and a net conversion gain⁷. Further details and performance characteristics of the PD-WC device can be found elsewhere⁸. Here we focus on the transmitter portion of the device which is comprised of a five section SG-DBR laser followed by an SOA for output amplification and a QW EAM consisting of seven 9.0 nm compressively strained wells and six 5.0 nm tensile strained barriers. The 5 sections of the SG-DBR laser are, from front to back of the laser: front mirror, gain, phase, rear mirror, and backside absorber, as depicted in Fig. 4. The phase and mirror sections function to tune the wavelength of the laser³. The output tuning spectra of the transmitter demonstrated over 40nm of continuous tuning with a side mode suppression ratio (SMSR) of > 35 dB at all wavelengths. The SG-DBR lasers demonstrated threshold currents of under 40mA with over 20 mW of output power at a gain current of 160 mA. There is no significant degradation in the laser performance over that of SG-DBRs fabricated using the offset QW platform, and in fact, there is a slight enhancement in the tuning efficiency of the lasers due to the addition of the QWs in the waveguide.



Fig. 4. Top view SEM of PD-WC using dual-QW platform and flared/tapered waveguide schemes in receiver.

In Fig. 5a, EAM extinction versus bias, and in Fig. 5b, EAM slope efficiency versus bias are presented for both bulk FK type EAMs fabricated using the offset QW method and QW EAMs fabricated using the dual QW method. The QW EAM provides up to 2.5X the efficiency than that of the FK device. Furthermore the QW EAM has an optimal operating bias regime in the 2.5 to 3.5V with respect to the extinction efficiency. The FK EAM demonstrates an increase in extinction efficiency at larger biases, requiring a larger modulation swing and resulting in relatively high on loss.

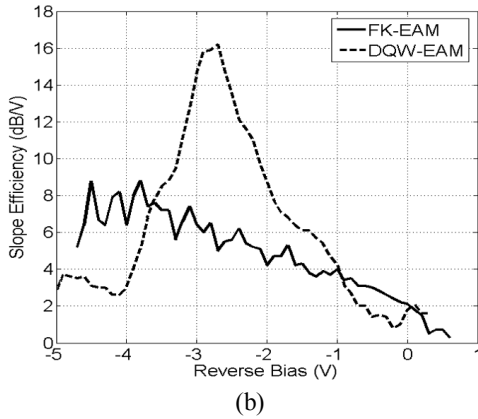
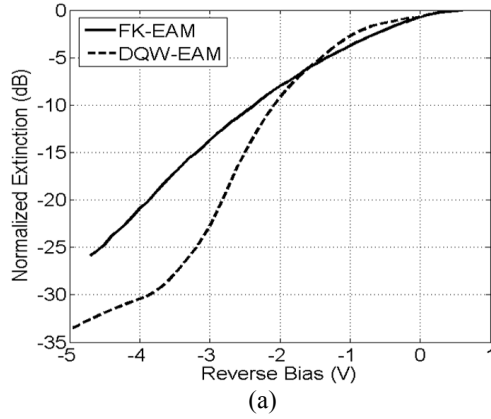


Fig.5 (a) Extinction and (b) slope efficiency versus reverse bias for 400 μm long EAMs employing the FK absorption mechanism fabricated on the offset QW platform and employing the QCSE absorption mechanism fabricated using the dual QW platform.

The reduced doping levels in the EAM required for optimized efficiency in the dual QW platform over that of the offset QW platform enables a significantly lowered device capacitance. As a result, a 400 μm long dual QW EAM demonstrating 10 GHz of 3 dB bandwidth, which is a factor of 2 better than the FK EAM response shown on the same plot. Thus, with the dual QW platform we have demonstrated a 2X improvement in EAM efficiency and bandwidth without any degradation to the laser performance or additional fabrication steps than those associated with the offset QW platform.

III.B. SG-DBR/EAM 10 Gb/s Transmitter Fabricated with QWI

Figure 6 shows results from a similar SGDBR-EAM transmitter fabricated with QWI with properties outlined in Fig. 3. This is the first widely-tunable transmitter demonstrating negative chirp characteristics at 10 Gb/s over its entire tuning range⁹. The SG-DBR laser demonstrated a threshold current of 13mA, with an output power of 10mW at a gain section current of 100mA. At this operating point, a side-mode suppression ratio (SMSR) greater than 35 dB was achieved. The EAM (175 μm) demonstrated over 40 dB of DC extinction for wavelengths of 1558, 1570, and 1580 nm, with efficiencies greater than 20 dB/Volt as shown in Fig. 6a.

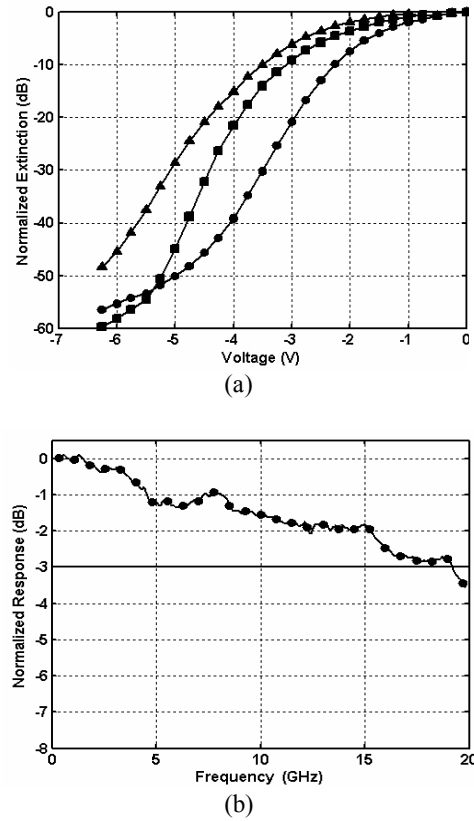


Fig. 6 (a) DC Extinction of a 175 μm EAM fabricated with QWI for wavelengths of 1558 nm (circles), 1570 nm (squares), and 1580 nm (triangles). And (b) electrical to optical frequency response of the same EAM. The circular markers represent every 30th data point.

The efficient extinction properties are due to the combination of the centered quantum well design and the intermixing process that allows for precise placement of the modulator band edge. The 3dB bandwidth, shown in Fig. 6b, of the same modulator was greater than 19 GHz. Eye diagrams, shown in Fig. 7a, were taken at wavelengths of 1558 nm, 1564 nm, 1571 nm, and 1578 nm with DC biases ranging from -2.1 to -

3.8 V and peak to peak voltage swings ranging from 2.2 V to 3.4 V. Greater than 10 dB extinction was achieved at all wavelengths.

Transmission experiments at 10 Gb/s were performed using a non-return to zero (NRZ) pseudo-random-bit-sequence (PRBS) of $2^{31}-1$ through Corning SMF-28 fiber. BER curves through 25, 50, and 75 km of fiber at a wavelength of 1564 nm are shown in Fig. 7b. The EAM was biased at -3.5 V with a 2.0 V peak-to-peak swing. Error-free operation was achieved through 75km of fiber with a power penalty of less than 0.5 dB. The low power penalty transmission is indicative of negative chirp operation²⁰. The shaping of the eye diagrams due to dispersion is clearly seen in the insets of Fig. 7b where the optical eye diagrams are shown after transmission through fiber.

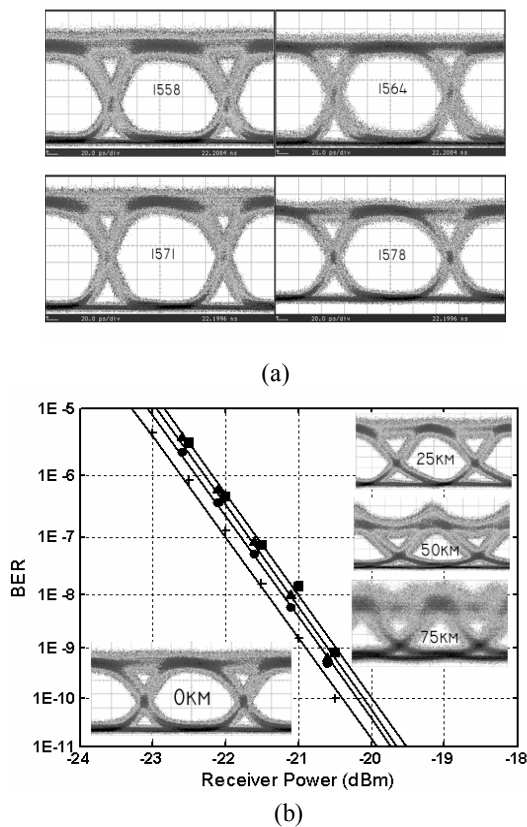


Fig. 7 (a) 10Gb/s back-to-back eye diagrams from transmitter at wavelengths of 1558 nm, 1564 nm, 1571 nm, and 1578 nm and (b) BER curves/eye diagrams for back-to-back (cross), and transmission through 25 km (circles), 50 km (triangles), and 75 km (squares) of fiber.

IV. Conclusion

The monolithic integration of optoelectronic components supporting modern day communication systems will provide solutions at low cost with a reduction of space requirements and device power dissipation. However, as the functionality of the PIC is increased, the challenge of realizing a high performance integrated is great due to the unique characteristics required by the individual components for optimum performance. To meet the increasing performance demands placed upon the PICs, novel integration platforms must be developed such that the design space is increased without significant increase in processing and growth requirements that can raise cost and lower yields.

We have reviewed two viable integration technologies, which provide the foundation for the monolithic integration of QW EAMs with widely tunable SG-DBR lasers. By growing a blue-shifted MQW in the bulk waveguide below the active MQW in the base structure, etching the active MQW in regions where gain is not required and performing a regrowth of the upper cladding, the dual QW platform requires the same simple processing/growth steps as the well-established offset QW platform with the added flexibility of a second MQW bandedge. By using our implant enhanced QWI scheme, any number of MQW band-edges can be realized on the same chip for the fabrication of high-functionality PICs. Furthermore, this method enables the use of a centered MQW active region for maximized modal gain lasers. Through the use of QWI, we have demonstrated the first widely-tunable negative chirp EAM based transmitter.

V. References

- [1] J. Binsma, P. Thijs, T. VanDongen, E. Jansen, A. Staring, G. VanDenHoven, and L. Tiemeijer, "Characterization of Butt-Joint InGaAsP Waveguides and Their Application to 1310 nm DBR-Type MQW Gain-Clamped Semiconductor Optical Amplifiers," *IEICE Trans. Electron.*, vol. E80-C, pp. 675-681, 1997.
- [2] M. Aoki, M. Suzuki, H. Sano, T. Kawano, T. Ido, T. Taniwatari, K. Uomi, and A. Takai, "InGaAs/InGaAsP MQW Electroabsorption Modulator Integrated with a DFB Laser Fabricated by Band-Gap Energy Control Selective Area MOCVD," *IEEE J Quantum Electron.*, vol. 29, pp. 2088-2096, 1993.
- [3] B. Mason, G. Fish, S. DenBaars, and L. Coldren, "Ridge Waveguide Sampled Grating DBR Lasers with 22-nm Quasi-Continuous Tuning Range," *IEEE Photon. Technol. Lett.*, vol. 10, pp. 1211-1213, 1998.
- [4] M. N. Sysak, J. W. Raring, D. J. Blumenthal, L. A. Coldren, "A Single Regrowth Integration Platform for Photonic Circuits Incorporating Tunable SGDBR Lasers, and Quantum Well EAMs," submitted to *Photonics Technology Letters*, 2006.
- [5] E. Skogen, J. Raring, J. Barton, S. DenBaars, and L. Coldren, "Post-Growth Control of the Quantum-Well Band Edge for the Monolithic Integration of Widely-Tunable Lasers and Electroabsorption Modulators," *IEEE J. Sel. Topics in Quantum Electron.*, vol. 9, pp. 1183-1190, September/October, 2003.

- [6] A. Tauke-Pedretti, M. Dummer, J.S. Barton, M.N. Sysak, J.W. Raring, and L.A. Coldren, "High Saturation Power and High Gain Integrated Photoreceivers," *IEEE Photon. Technol. Lett.*, vol. 17, pp. 2167-2169, 2005.
- [7] M. N. Sysak, J. W. Raring, J. S. Barton, M. Dummer, A. Tauke-Pedretti, H. N. Poulsen, D. J. Blumenthal, L. A. Coldren, "10 Gb/s Photocurrent Driven, Electroabsorption Modulator Based Wavelength Converter with Monolithically Integrated Widely Tunable SGDBR Laser and Optical Receiver," accepted for presentation at the Integrated Photonics Research Conference, 2006.
- [8] J. S. Barton, A. Tauke-Pedretti, M. Dummer, M. N. Sysak, J. W. Raring, L. A. Coldren, "Field Modulated Wavelength Conversion, *Invited*, 6124 -42. San Jose, CA, January 21-26, 2006.
- [9] J. Raring, E. Skogen, L. Johansson, M. Sysak, S. DenBaars, and L. Coldren, "Widely-Tunable Negative-Chirp SG-DBR Laser/EA-Modulated Transmitter," *IEEE Journal of Lightwave Technology*, vol. 23 no.1, pp. 80-86, Jan. 2005.